THE JOURNAL OF PHYSICAL CHEMISTRY C

Article

Cite This: J. Phys. Chem. C 2018, 122, 2173−2183

pubs.acs.org/JPCC

Combined TPD and XPS Study of Ligation and Decomposition of 1,6-Hexanedithiol on Size-Selected Copper Clusters Supported on HOPG

Linjie Wang,[†] Nicolas Blando,[†] Zachary Hicks,[†] Michael Denchy,[†] Xin Tang,[†] Hannes Bleuel,[‡] Mingshi Zhang,[†] Gerd Ganteför,[‡] and Kit H. Bowen*[,†]

[†]Department of Chemistry, Johns Hopkins University, Baltimore, Maryland 21218, United States

[‡]Department of Physics, University of Konstanz, Konstanz 78457, Germany

ABSTRACT: Ligation and decomposition of 1,6-hexanedithiol on copper clusters have been studied by means of temperature-programmed desorption (TPD) and X-ray photoelectron spectroscopy (XPS). Copper cluster anions were first made via magnetron sputtering, then size selected and soft landed into a frozen matrix of 1,6-hexandithiol on highly ordered pyrolytic graphite (HOPG) maintained at 100 K. After warming up to 298 K, a combination of TPD and XPS were performed to characterize the newly deposited sample. TPD data shed light upon the adsorption and decomposition pathways of 1,6-hexanedithiol molecules on copper clusters. Based on the TPD data, two different binding motifs are proposed: the dangling motif is with one sulfur atom binding to a copper cluster, and the bidentate motif is with both sulfur atoms binding to a copper cluster. Different decomposition products were observed for each binding motif. A series of hydrogen atom titration experiments were designed to provide further evidence for the proposed decomposition mechanism. XPS measurements at varied temperatures agree well with the TPD profile by confirming the formation of dithiol ligated copper clusters through Cu−S bond formation, and the decomposition of them via C−S bond scission. How well the dithiol ligand can protect the copper clusters from being oxidized is discussed, and the ligand number per cluster is estimated.

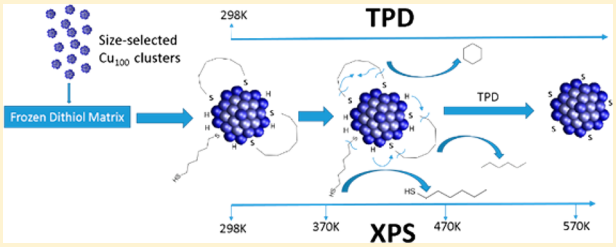

INTRODUCTION

Exploring and understanding the catalytic properties of ultrasmall metal clusters are of great significance not only in academia but also in industry. Ultrasmall metal clusters, which have high surface to volume ratios and a high percentage of low-coordinated metal atoms on the surface, have unique physical and chemical properties that are distinct from their macroscopic counterparts. Numerous studies have highlighted the ability of the cluster deposition method to explore the catalytic reactivity of ultrasmall clusters with different sizes, contents, and substrates.[1] Pioneering work on size selected Au_n and Pt_n clusters deposited on a Si(100) wafer by the Exxon group marked the emergence of this cutting-edge research field.[2] From then on, a lot of studies have been focusing on size selected noble metals such as Pt_n,[3,4] Pd_n,[5−7] Ag_n,[8−10] and Au_n.[11−14] Copper, a readily available and less expensive catalyst, also served as a promising candidate in this field. For example, size-selected Cu_4 clusters supported on Al_2O_3 thin films have demonstrated promising catalytic activity toward the activation of CO_2 and its hydrogenation to methanol.[15]

Atomic sulfur is well-known to poison the surface of many catalysts.[16−18] Adsorption studies of sulfur-containing molecules on different transition metal surfaces are of great interests to both catalytic and surface chemists.[19] There have been comprehensive adsorption studies for alkanethiols, especially the simplest methanethiol, on different metal single crystal surfaces.[20−26] There have also been studies of longer carbon chain monothiols especially on Cu single crystal surfaces.[27,28] However, studies on interactions between ultrasmall copper clusters and alkanethiols using surface science techniques under ultrahigh vacuum (UHV) are rare. Moreover, studies on bifunctional and longer carbon chain alkanethiols, such as 1,6-hexanedithiol, interacting with ultrasmall copper clusters are even rarer.

Using inorganic synthesis and material science approaches, long alkanethiols, as well as complex thiol group containing organics, have been effectively used as capping agents for various nanoparticles.[29−32] It is reasonable to expect that the alkanethiols may behave differently with copper clusters in a wet chemistry solution phase than in a surface science UHV environment. Only recently, Whitten et al. have carried out a comparison study between colloidal copper oxide particles and oxidized copper single crystal surfaces, exploring the adsorption of thiols and reduction of copper oxides.[33] However, studies on the formation and decomposition of alkanethiol ligated copper clusters from a surface science perspective are still rare.

In this study, we use the size-selected cluster deposition method to study the interactions between ultrasmall copper clusters of desired size and 1,6-hexanedithiol molecules. 1,6-Hexanedithiol is chosen because of its bifunctional and six-

Received: October 23, 2017
Revised: December 16, 2017
Published: January 3, 2018

DOI: 10.1021/acs.jpcc.7b10452
J. Phys. Chem. C 2018, 122, 2173−2183

membered carbon chain structure, which may result in unique adsorption and decomposition properties. In most studies on the catalytic properties of size-selected metal clusters, defect rich surfaces or metal oxide thin films that can interact strongly with the as-deposited metal clusters are chosen as substrates. This is because they can offer preferred metal cluster binding sites, effectively pinning the clusters to the surface and inhibiting agglomeration.[1,10,14,34] However, in this study, the inert and super flat HOPG surface is chosen to reduce cluster−substrate interactions. To also reduce the cluster−cluster interactions and promote the cluster−ligand interactions, size-selected copper clusters are deposited into a frozen matrix of 1,6-hexanedithiol formed on the HOPG substrate maintained at 100 K. This method is originally inspired by the common experimental technique used in the matrix isolation infrared spectroscopy.[35] Generally, noble gases such as argon are chosen to form a hosting matrix because of their inert nature as well as broad optical transparency. Using this matrix isolation technique, short-lived, highly reactive species can be trapped and analyzed by spectroscopic means.[36−38] This method was later adopted to probe the activities of metals or metal oxides toward a reactive matrix.[39−43] For instance, $(MoO_3)_3$ or $(WO_3)_3$ clusters were deposited into a reactive matrix of ethanol to study the clusters' dehydration and oxidation properties toward ethanol.[44] A graphene thin film over Pt(111) was chosen as an inert substrate not only for its unreactivity toward alcohols, but also to minimize the substrate's effects on the acidic and redox properties of those metal oxide clusters.[44] In this study, we adopted a similar idea by freezing a reactive matrix of 1,6-hexanedithiol onto an inert HOPG substrate. After deposition, the HOPG substrate was warmed up to 298 K, when dithiol ligated copper clusters were believed to form. Then, temperature-programmed desorption (TPD) and X-ray photoelectron spectroscopy (XPS) were carried out to characterize the adsorption and decomposition properties of 1,6-hexanedithiol on copper clusters.

EXPERIMENTAL METHODS

Copper clusters Cu_n^- were prepared as negative anions by a magnetron sputtering source. After acceleration, mass selection and deceleration, they were then deposited (soft-landed) onto a piece of HOPG (Bucker, ZYB grade, 1.2 × 1.2 mm^2, 2 mm thickness) under ultrahigh vacuum (base pressure 1 × 10^{-9} Torr). The whole setup was described in detail elsewhere.[45]

The magnetron setup consisted of a copper sputtering target (99.99%) placed in a magnetic field and biased to −500 V when a mixture of argon (Airgas, 99.999%) and helium (Airgas, 99.999%) was introduced. The argon gas was ionized to create argon cations, which sputtered the metal target to produce a plasma. The added helium served to cool and transport the cluster anions down the beamline, where they were then electrostatically accelerated before entering a magnetic sector mass spectrometer (25° sector magnet with resolution of $m/\Delta m$ = 20). By tuning the magnetic field strength, a beam of Cu_n^- (for Cu_{100}^-, n = 100 ± 5) cluster anions was mass-selected and focused by ion optics into the deposition chamber, where they were soft-landed (<1 eV) onto a piece of freshly peeled and annealed HOPG. The resulting sample could be cooled down to approximately 100 K by liquid nitrogen (LN_2) or heated up via resistive heating to 720 K. The temperature of the sample was monitored by a K-type thermocouple spring loaded to the back of the HOPG.

Dithiol ligated copper clusters were made via the liquid nitrogen matrix deposition method (LNMD method). HOPG samples were cleaved in air right before being transported into the vacuum chamber and then annealed at 720 K for 30 min before use. 1,6-Hexanedithiol (96%) purchased from Sigma-Aldrich was degassed by three freeze−pump−thaw cycles before being introduced into the vacuum chamber through a UHV compatible leak valve. For the LNMD method, the dithiol was dosed into the chamber when the HOPG had already been cooled down to and held at 100 K, forming multilayers on the HOPG. The dose of the dithiol was monitored by a pressure gauge and a residual gas analyzer (RGA) (Hiden HAL/3F PIC quadrupole mass spectrometer (QMS)). And the dose amount was given in Langmuir (L, 10^{-6} Torr·s). After dosing, size selected copper clusters were deposited into that premade frozen dithiol matrix. During a deposition, the deposition current was monitored by a picoammeter, and the coverage of the as-deposited clusters was given in current (ampere, A) integrated over time (second, s). For each deposition, the average deposition current was about 70 pA, corresponding to an average deposition speed of 4 × 10^8 clusters per second; and the final deposition amount was controlled to be 1 × 10−6 A·s, corresponding to the total amount of 6 × 10^{12} clusters on a 1.2 × 1.2 cm^2 substrate. After deposition, the sample was ramped up from 100 to 298 K by resistive heating.

Once warmed up to 298 K when the dithiol ligated copper clusters were believed to have formed, TPD was used to characterize the dithiol's decomposition properties on copper clusters. The desorption products were detected and identified by a QMS, which was positioned normal to the plane of the substrate at a distance of about 5 mm. Also, the entrance of the QMS is covered by a glass shroud with a 6 mm diameter hole cut at the center. These two configurations can both help to minimize the contributions from background gases and maximize the sensitivity toward the species desorbing directly from the substrate. With regard to the customized TPD sample holder, two small pieces of tantalum foil are wrapped on two copper power feedthroughs respectively for resistive heating purposes, and a piece of HOPG is held between them.

The as-prepared dithiol ligated copper clusters were also characterized via ex situ XPS with nonmonochromatic Mg Kα rays (1253.6 eV), and the kinetic energies of ejected electrons were analyzed via a high energy hemispherical analyzer. To accomplish this, the sample needed to be taken out of the deposition chamber and then transferred into an adjacent chamber dedicated to XPS. For XPS measurements at varied temperature, the sample was heated in situ via e-beam heating to the desired temperatures and then cooled back down to about 300 K, at which XPS spectra were recorded. All the XPS spectra were calibrated by graphitic carbon 1s at 284.5 eV.[46] Sulfur XPS spectra were numerically fitted with the Gaussian broadened Lorentzian function (LF(1,1,25,280)) after a Shirley background subtraction in CasaXPS (Casa Software Ltd.). S 2p spin−orbit splitting doublets were composed of two components separated by 1.18 eV with an integrated area ratio of 1:2.[24] Full width at half-maximum (fwhm) were controlled in a range of 3.5−4 eV depending on the surface species when using a pass energy of 178.95 eV. For each oxidation state, consistent binding energy range constraints, intensity ratio and fwhm were kept the same across each temperature dependent XPS spectrum.

DOI: 10.1021/acs.jpcc.7b10452
J. Phys. Chem. C 2018, 122, 2173−2183

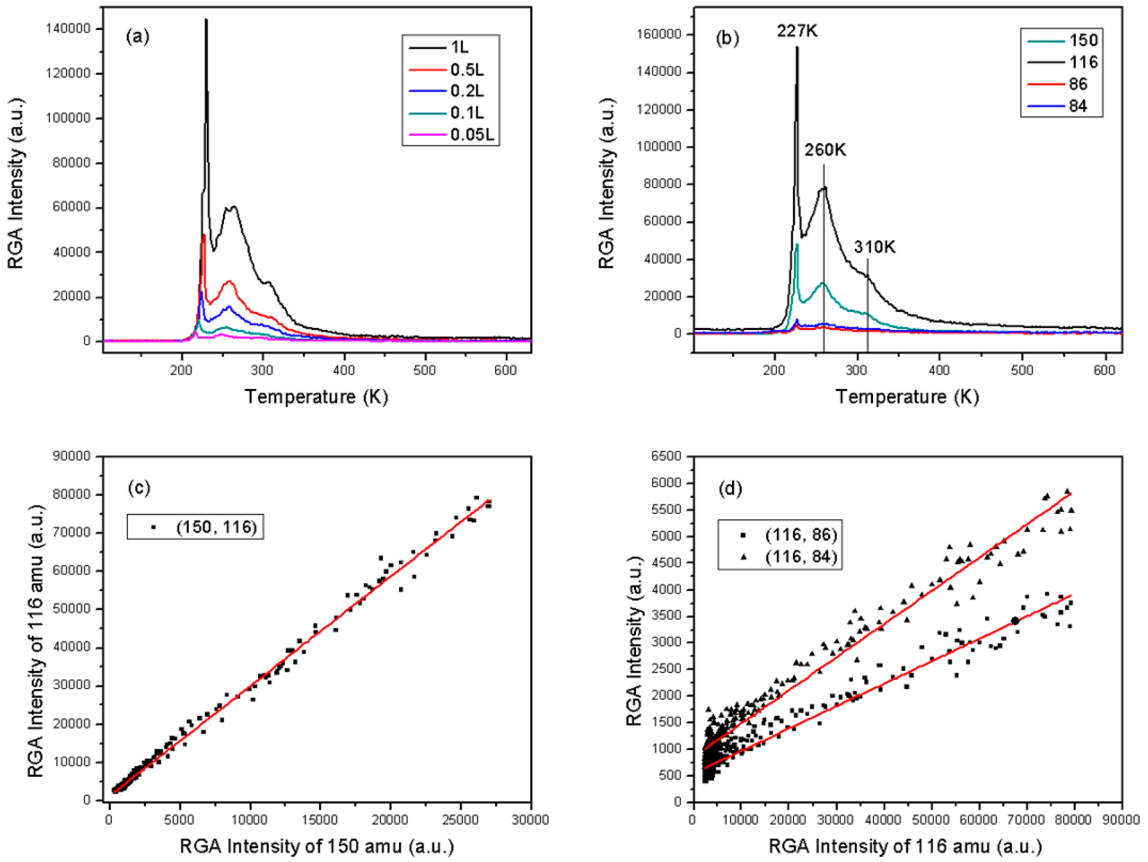

Figure 1. TPD profile of 1,6-hexanedithiol physical desorption on HOPG substrate. (a) TPD scans of molecular dithiol (m/e = 150) as a function of dose amount; (b) Composite TPD scans of 0.5L dose: molecular dithiol (m/e = 150), monothiol (m/e = 116), hexane (m/e = 86) and cyclohexane (m/e = 84); (c) (■) RGA intensity of the monothiol plotted to that of the molecular dithiol, red line is the linear fitting (slope: 2.97 ± 0.01, intercept: 1380 ± 80, R^2: 0.996); (d) (■) RGA intensity of hexane plotted to that of the monothiol and the corresponding linear fitting (slope: 0.0422 ± 0.0005, intercept: 553 ± 11, R^2: 0.96), (▲) RGA intensity of cyclohexane plotted to that of the monothiol and the corresponding linear fitting (slope: 0.0648 ± 0.0006, intercept: 866 ± 14, R^2: 0.97).

RESULTS AND DISCUSSION

1,6-Hexanedithiol Reaction Pathway on Copper Clusters. The reaction pathways of 1,6-hexandithiol on copper clusters were studied via TPD. HOPG has been used as an inert carbon substrate to study the desorption energetics of alkane derivatives as well as the catalytic reactivity of clusters through TPD.[47−49] There are also STM and AFM studies on self-assembly of organic molecules using HOPG as an inert substrate.[50] However, there are not many TPD studies on the desorption energetics of alkanethiols. The LNMD method requires formation of a dithiol matrix; however, most of the dithiols are just physisorbed on the HOPG surface due to the low intensity of the cluster deposition. Therefore, the physisorption properties of 1,6-hexanedithiol on HOPG without copper clusters was studied via TPD initially.

Figure 1 shows the TPD profile of 1,6-hexandithiol desorption from HOPG without copper clusters. Figure 1a shows the TPD spectra of intact dithiol (m/e = 150) with varied dose amount. For a dose larger than 0.2L, there are apparently three features, each of which is associated with dithiol molecules desorbing from a different surface layer. At the lowest temperature (230 K), there is an intense, sharp peak due to multilayers' desorption; a broad peak lies in a slightly higher temperature range (∼260 K) representing the monolayer; also note that there is a less intensive shoulder possibly coming from the sample holder at a slightly higher temperature (∼310 K). As the dose amount decreases, the first two peaks shift to lower temperatures with lower intensity, suggesting a zeroth order physical desorption. Also note that even when the dose is decreased to 0.05L, the multilayer peak still exists and that for increasing dose amounts, the monolayer peak does not seem to be saturated when the multilayer peak is already very strong. These two features suggest that the adsorbates may grow according to a Volmer−Weber mechanism rather than a layer-by-layer mode.[51] In other words, multilayers tend to form when a monolayer has not formed completely. The similar mechanism has also been proposed to explain acetone adsorption on HOPG based on experimental and theoretical investigations.[52]

The dose amount was maintained at 0.5L for the rest of the TPD experiments for better consistency. Figure 1 (b) shows a composite TPD scan collected from a dose of 0.5L. Monothiol (m/e = 116) is one of the major fragments of 1,6-hexanedithiol through desulfurization, while hexane (m/e = 86) and cyclohexane (m/e = 84) are not the major fragments based on the relatively low RGA intensity. Linear fittings shown in Figure 1c and d by RGA intensity of the fragments versus that of the intact dithiol reveal that the fragmentation pattern remains constant for the whole desorption process, indicating that neither the HOPG substrate nor the sample holder causes obvious decomposition of the dithiol molecules.

DOI: 10.1021/acs.jpcc.7b10452
J. Phys. Chem. C 2018, 122, 2173−2183

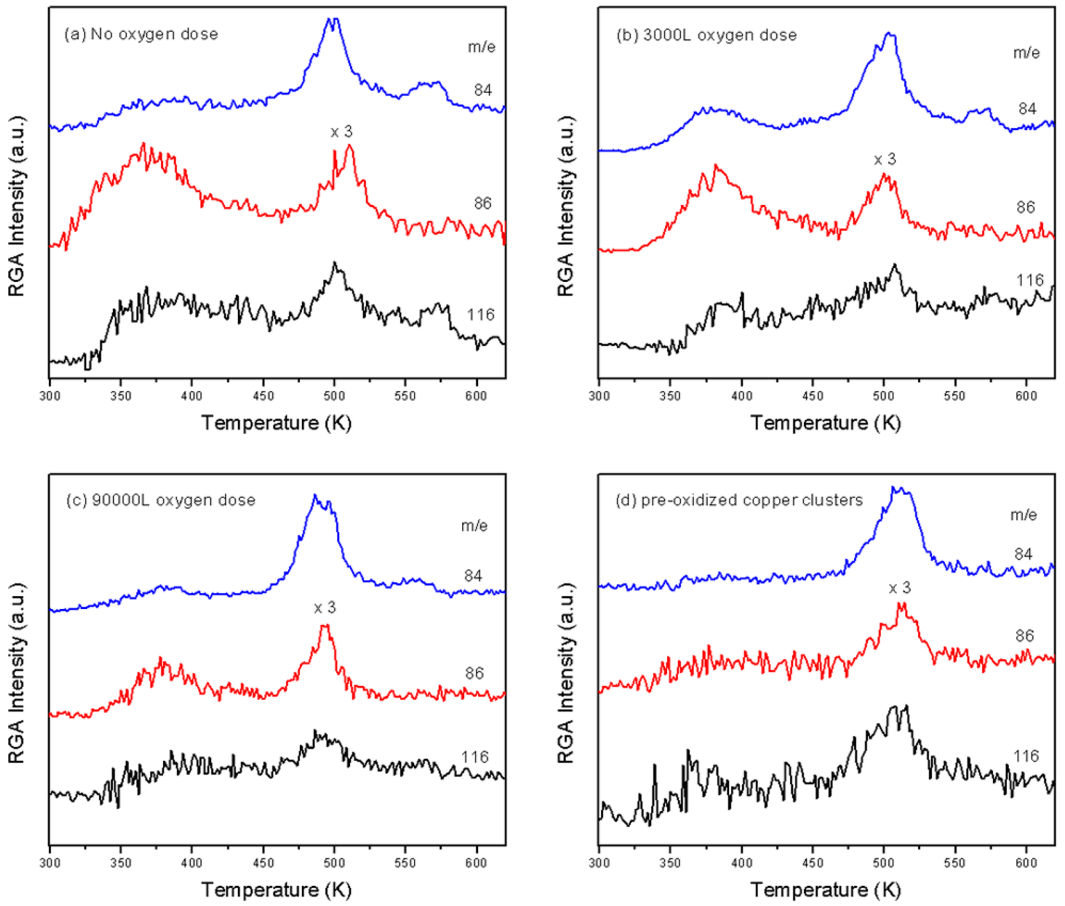

Figure 2. Composite TPD spectra of dithiol ligated clusters under different oxygen conditions: (a) Cu_{100} without dosing oxygen; (b) Cu_{100} with 3000L oxygen dosing; (c) Cu_{100} with 90000L oxygen dosing; (d) $(CuO)_{80}$ without dosing oxygen.

For an experimental TPD scan, data cannot be collected from 100 K all the way to 700 K, because the intensive physi-desorption signals would overwhelm the desorption peaks caused by the copper clusters. A compromising solution is to ramp up to 298 K first, and remain there for 30 min to remove any physisorbed dithiol, then collect the TPD spectra from 298 to 700 K. As is shown in Figure 2a, it is identified that monothiol (m/e = 116), hexane (m/e = 86) and cyclohexane (m/e = 84) are the major volatile products that desorb upon heating. There are three desorption temperature regions: a low temperature region in the 350−420 K range, a medium temperature region in the 460−540 K range, and a high temperature region in the 540−600 K range. In each region, there is a different combination of the three desorption products. It should be mentioned that before each deposition, a background scan was carried out to make sure that there was no obvious peak in the 350−600 K temperature region, and also to obtain the fragmentation ratios which were later on used to subtract the contributions due to ionization fragmentation of the intact dithiol molecules.

In the low temperature region, hexane is the major desorption product. There is also a rising terrace for the monothiol, part of which may be due to a rising background. However, the cyclohexane peak is too weak to be discernible from the background. In the medium temperature range, all three decomposition products are observed, among which cyclohexane is the major product. In the high temperature region, there is no peak for hexane, but two small peaks for cyclohexane and monothiol. Comparing these three temperature regions and their respective desorption species, the following can be established: 1. The medium temperature region is the major desorption region because of the higher intensity of desorption peaks, as well as the existence of all three decomposition species; 2. Monothiol is the only species that desorbs in all three temperature regions; 3. Both hexane and cyclohexane evolve in two consecutive temperature regions; 4. Hexane is likely to form in a relatively lower temperature range, while cyclohexane tends to evolve in a relatively higher temperature range; 5. Every temperature region has at least two desorption species, the peak positions of which coincide with each other very well.

Monothiol (m/e = 116) can get fragmented to produce an ion with an m/e of 86 or 84 by electron bombardment in the ionization zone of a QMS. However, the evolution of m/e = 86 and m/e = 84 do not really follow that of m/e = 116 as is shown in Figure 2a. Moreover, as the linear fitting in Figure 1d illustrates, the percentages of m/e = 116 that can fragment into ion species of m/e = 86 or m/e = 84 due to electron bombardment are very limited (less than 7% percent). Based on these two facts, even though the peaks of m/e = 86, 84, and 116 appear coincident, the evolutions of m/e = 86 and 84 are from decomposition of dithiol on copper clusters instead of fragmentation of m/e = 116 in the ionization zone.

The proposed adsorption and decomposition mechanism of 1,6-hexanedithiol is shown in Scheme 1. First, size selected copper clusters (Cu_n^-, n = 100 ± 5) are deposited into a premade 1,6-hexanedithiol frozen matrix. Second, while ramping up to room temperature, dithiol molecules either

DOI: 10.1021/acs.jpcc.7b10452
J. Phys. Chem. C 2018, 122, 2173−2183

Scheme 1. Formation of 1,6-Hexanedithiol Ligated Copper Clusters and the Decomposition of 1,6-Hexanedithiol on Copper Clusters

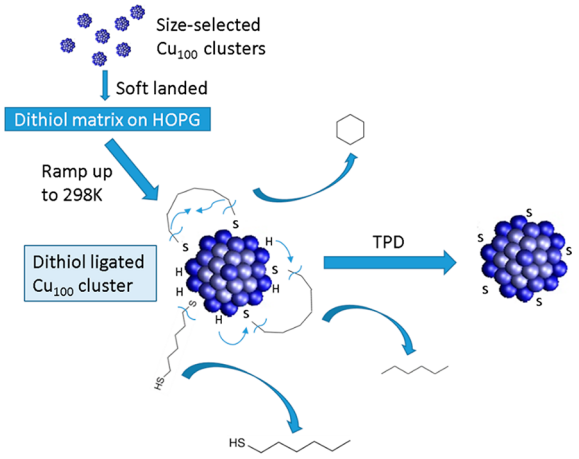

chemisorb to the copper clusters via S−H bond scission and Cu−S bond formation, or physi-desorb from HOPG. Since a 1,6-hexanedithiol molecule has two thiol groups, it can anchor to a copper cluster with one end forming a dangling dithiol (eq 1) or with both ends forming a bidentate dithiol (eq 2). Third, during a TPD ramp, the chemisorbed dithiol molecules undergo decomposition via C−S bond scission. A dangling dithiol will lose one sulfur after C−S bond scission and form a six-carbon monothiol (eq 3), while a bidentate dithiol will either recombine with two adsorbed hydrogen atoms to form hexane (eq 4) or undergo intramolecular coupling to form cyclohexane (eq 5). Finally, only atomic sulfur atoms remain on the copper clusters.

$$HSC_6H_{12}SH(a) \rightarrow HSC_6H_{12}S(a) + H(a) \quad (1)$$

$$HSC_6H_{12}SH(a) \rightarrow SC_6H_{12}S(a) + 2H(a) \quad (2)$$

$$HSC_6H_{12}S(a) \rightarrow HSC_6H_{12}(g) + S(a) \quad (3)$$

$$SC_6H_{12}S(a) + 2H(a) \rightarrow C_6H_{14}(g) + 2S(a) \quad (4)$$

$$SC_6H_{12}S(a) \rightarrow C_6H_{12}(g) + 2S(a) \quad (5)$$

$$2H(a) \rightarrow H_2(g) \quad (6)$$

This decomposition mechanism is proposed based on the TPD spectra of our supported copper clusters system and also the literature about the monothiol copper single crystal system. From the point of view of surface science studies, the simplest monothiol, methanethiol, has been the starting point of studies on interactions between thiols and copper single crystal surfaces.[19] Adequately high resolution XPS measurements and HREELS spectra have identified the main surface species as an intact, physisorbed molecule at the lowest temperature (~80 K); a surface thiolate, i.e., methyl mercaptide, produced by deprotonation at slightly higher temperatures (still lower than room temperature); the formation of atomic sulfur via C−S bond scission and the evolution of hydrocarbon products occur at temperatures higher than 300 K.[19,23] Combined TPD studies have identified the evolution of methane formed via recombination of adsorbed hydrogen, ethane formed via intermolecular coupling, ethene formed via coupling and C−H bond scission, as well as H_2 formed via recombination of adsorbed hydrogen atoms.[19,24,25]

Compared to single crystal studies, hexane observed in our system is speculated to evolve through the similar hydrogen recombination reaction pathway. In terms of coupling reactions, Hung et al. have found that intermolecular coupling of alkyl groups is not observable for C_2H_5SH and C_4H_9SH, in contrast with CH_3SH.[24] They attribute that to the possibility that longer alkyl groups might diffuse along the surface with greater difficulty, or the molecular orientation for coupling may be restrictive.[24] In our system, instead of undergoing intermolecular coupling, ideal carbon chain length and bifunctional nature make it more feasible for 1,6-hexanedithiol to form a stable six-membered ring via intramolecular coupling. With both sulfur atoms binding to copper clusters through a bridge structure, the two ends are forced to stay close to each other for facile coupling without the necessity of diffusion.

As explained above, ionization induced fragmentation has been ruled out for causing the coincidence of desorption peaks. Also note that thermally induced C−S scission is the elementary reaction step involved in the evolution of all three desorption products. Hence, it is speculated that C−S scission is the rate-limiting step for the evolution of all three desorption products.

Adsorbed Hydrogen Atom Titration. As was summarized for Figure 2a previously, hexane is likely to evolve in a relatively lower temperature range, while cyclohexane tends to desorb in a relatively higher temperature range. Considering the hydrogen recombination mechanism for the evolution of hexane, it is speculated that this phenomenon is caused by the fact that the amount of adsorbed hydrogen decreases during the ramp of temperature. In the low temperature region, there are plenty of adsorbed hydrogen, resulting in preferential formation of hexane; in the medium temperature region, when there is significantly less adsorbed hydrogen, cyclohexane becomes prevalent; in the high temperature region, the adsorbed hydrogen atoms have all undergone either C−H formation (eq 4) or H−H formation (eq 6), making it impossible for hexane to evolve, but still possible for cyclohexane or monothiol to evolve.

To provide more evidence for this proposed mechanism, a series of hydrogen atom titration experiments have been designed. For a typical titration TPD scan, the sample was held at 298 K and oxygen was background introduced into the vacuum chamber via a UHV compatible leak valve. The purpose of this titration experiment is to use dosed oxygen to react with and then remove the adsorbed hydrogen atoms. And the effects of this titration process should be revealed in the TPD ramp afterward. Background experiments have also been done with the same amount of oxygen dosing but no deposited copper clusters, and there is no obvious peak in the 350−600 K range (data not shown here), which is very similar to the TPD with dosing the dithiol only.

Qualitative changes in the TPD spectra were observed when 3000L of oxygen was background dosed at 298 K. As is shown in Figure 2b, the major change occurred in the low temperature region, namely, the appearance of a small, broad peak of cyclohexane coinciding with that of hexane. Figure 3a and b show a better comparison between the runs without and with dosing oxygen for solely cyclohexane. A reasonable explanation for this phenomenon is that the dosed oxygen can titrate some of the adsorbed hydrogen atoms. As a result, in the low temperature region, not all of the bidentate dithiols have a chance to recombine with hydrogen atoms and then form hexane. Hence, some of the dithiol species will undergo

DOI: 10.1021/acs.jpcc.7b10452
J. Phys. Chem. C 2018, 122, 2173−2183

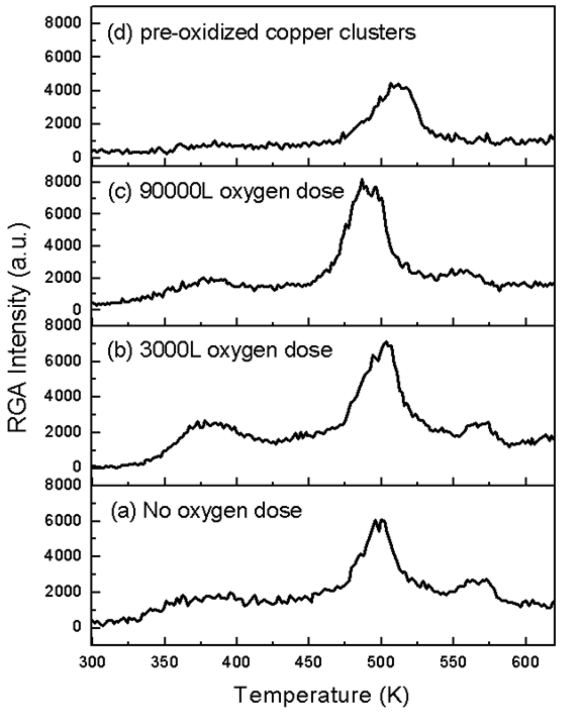

Figure 3. TPD scans of cyclohexane (m/e = 84) collected from 1,6-hexanedithiol ligated clusters supported on HOPG under different oxygen conditions.

intramolecular coupling and form cyclohexane. In other words, dosing 3000L of oxygen at 298 K can titrate the adsorbed hydrogen atoms partially, thus making hydrogen recombination and intramolecular coupling the two competing reaction pathways for the bidentate dithiol binding motif in the low temperature region.

If we follow this idea, it seems reasonable to expect that increasing the amount of dosed oxygen can eventually titrate almost all of the adsorbed hydrogen atoms such that hexane may disappear from the TPD spectra. However, it turned out not to be the case. Figure 3c shows that, after a significantly larger amount of oxygen (900 000L) being background dosed into the chamber, the low temperature peak for cyclohexane becomes weaker compared to that in Figure 3b. In fact, it almost disappears and becomes comparable to the peak from the TPD spectrum without an oxygen dose shown in Figure 3a. Also note that the medium temperature peak for cyclohexane gets larger and broader, while the high temperature peak becomes less discernible from the background. Additionally, for hexane, the low temperature peak gets weaker compared to the medium temperature peak. In general, a larger oxygen dose causes a redistribution of desorption products from the low and high temperature regions to the middle temperature region.

In fact, dosed oxygen can not only titrate adsorbed hydrogen but also form chemisorbed oxygen on copper clusters. With a relatively small amount of oxygen (3000L), the main effects revealed in the TPD spectra is its partial titration effects. However, with a larger amount of oxygen (90 000L), after some adsorbed hydrogen atoms being titrated, the copper clusters can start to become oxidized. Small clusters, such as Cu_{100}, can have their chemical properties and electronic structures perturbed as a result of oxidation on the surface. And these perturbations can have discernible influences on the TPD spectra. The evolution of desorption peaks from Figure 2b to c indicates that the effects stemming from oxidation of copper clusters with a large oxygen dose may overwhelm the effects of partial hydrogen titration, which should be revealed with a relatively small amount of oxygen otherwise. To gain more evidence to support this uncertain statement, a pre-oxidation experiment was carried out. Unlike the titration experiment, in which oxygen was introduced after the ligation process; for this pre-oxidation experiment, we made copper oxide cluster anions by introducing oxygen into the magnetron source, then $(CuO)_{80}^-$ (same m/e as Cu_{100}^-) was mass selected, and finally deposited into the frozen dithiol matrix. Therefore, copper clusters were oxidized first, and then got ligated by dithiol molecules.

As is shown in Figure 2d, the $(CuO)_{80}$ dithiol TPD spectrum has only one desorption region, which is close to the medium temperature region shown in Figure 2a–c. This means that, unlike Cu_{100}, which has three very different groups of binding sites; on $(CuO)_{80}$ clusters, there is only one group of binding sites, the sulfur binding energies of which are similar to that of the binding sites corresponding to the medium temperature region for Cu_{100}. Moreover, the peaks of the three major desorption species coincide with each other very well, indicating that C–S bond scission is also the rate limiting step for decomposition and desorption of the adsorbed dithiol on $(CuO)_{80}$ clusters.

As for now, there is a series of TPD experiments with different oxygen effects: without oxygen, a small amount of oxygen, a large amount of oxygen and pre-oxidation. Since the pre-oxidation one is with oxidized copper clusters, it can be seen as the maximum dosing amount of oxygen. For the three desorption products, Figures 3–5 show the evolution of each species under different oxygen conditions, sorted (bottom to top) in order of increasing oxygen amount. As oxygen amount increases, the changes occur mainly in the low temperature

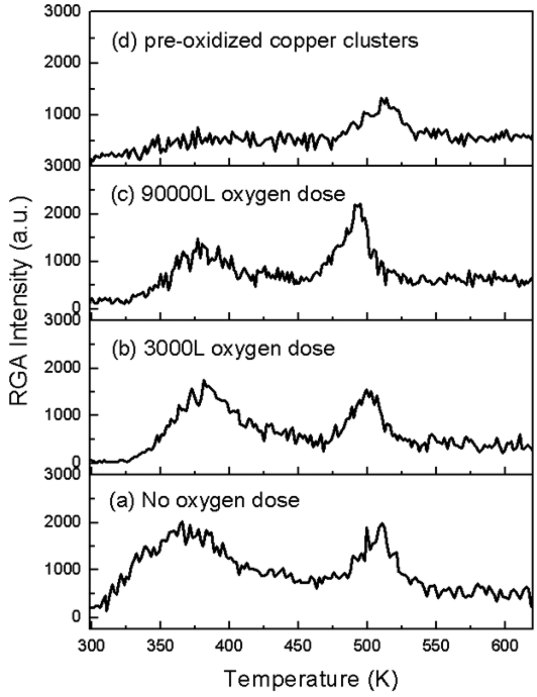

Figure 4. TPD scans of hexane (m/e = 86) collected from 1,6-hexanedithiol ligated clusters supported on HOPG under different oxygen conditions.

DOI: 10.1021/acs.jpcc.7b10452
J. Phys. Chem. C 2018, 122, 2173–2183

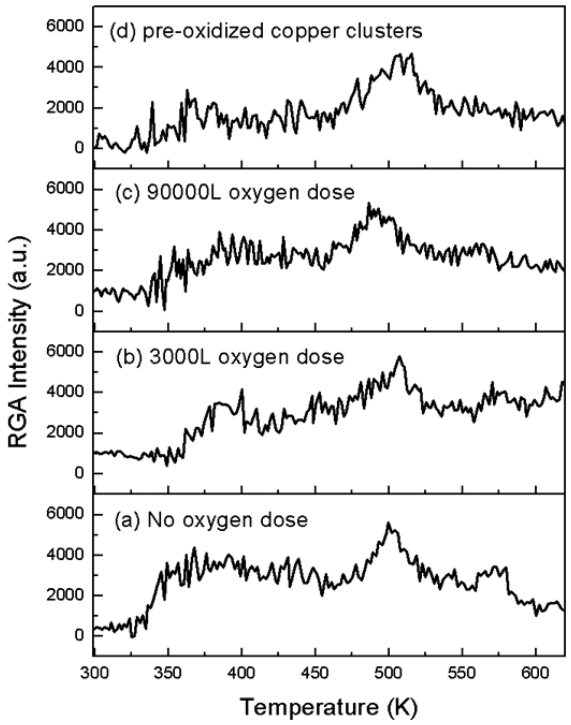

Figure 5. TPD scans of the monothiol (m/e = 116) collected from 1,6-hexanedithiol ligated clusters supported on HOPG under different oxygen conditions.

region for hexane and cyclohexane. For hexane, the intensity of the peak in the low temperature region gradually decreases until it finally disappears. For cyclohexane, a weak and broad peak appears with a small amount of oxygen, and then becomes weaker until finally disappearing. Based on the evolution of TPD spectra for hexane and cyclohexane, it is likely that with a small oxygen dosing amount such as 3000L, the TPD spectra reveal the partial hydrogen titration effects, and that with a larger oxygen dosing amount such as 90000L, the TPD spectra reveal mainly the oxidation effects.

XPS Characterization. Surface species formed upon ligation and left behind after annealing on Cu clusters were identified chemically using XPS. Figure 6 shows the spectra of S 2p sorted (bottom to top) in order of increasing annealing temperature. In the case of 298 K, the binding energy of S $2p_{3/2}$ is observed predominantly at 162.6 eV, which is attributed to the thiolate group (Cu−S−R). The higher binding energy peak at 167.3 eV indicates that some thiol groups get oxidized when exposed to air. No obvious oxidation state at around 164−165 eV is observed, which would be assigned to intact thiol groups. Therefore, it is speculated that some thiol groups from the dangling ligands may be oxidized or chemisorbed to the oxidized copper clusters.

As is shown in Figure 6 from (a) to (d), the major envelope peak position gradually shifts to lower binding energy. Deconvoluted peaks reveal three different oxidation states: 161.5, 162.6, and 167.3 eV, refering to sulfur oxidation states in Cu−S, Cu−S−R, and SO_2, respectively. From 298 to 570 K, the peak of S $2p_{3/2}$ at 162.6 eV due to Cu−S−R gradually disappears as a result of C−S bond scission. Meanwhile, the peak of S $2p_{3/2}$ at 161.5 eV increases, indicating the formation and accumulation of atomic sulfur atoms on the copper clusters. At 570 K, no obvious 162.6 eV component exists, implying that all the Cu−S−R species have decomposed and

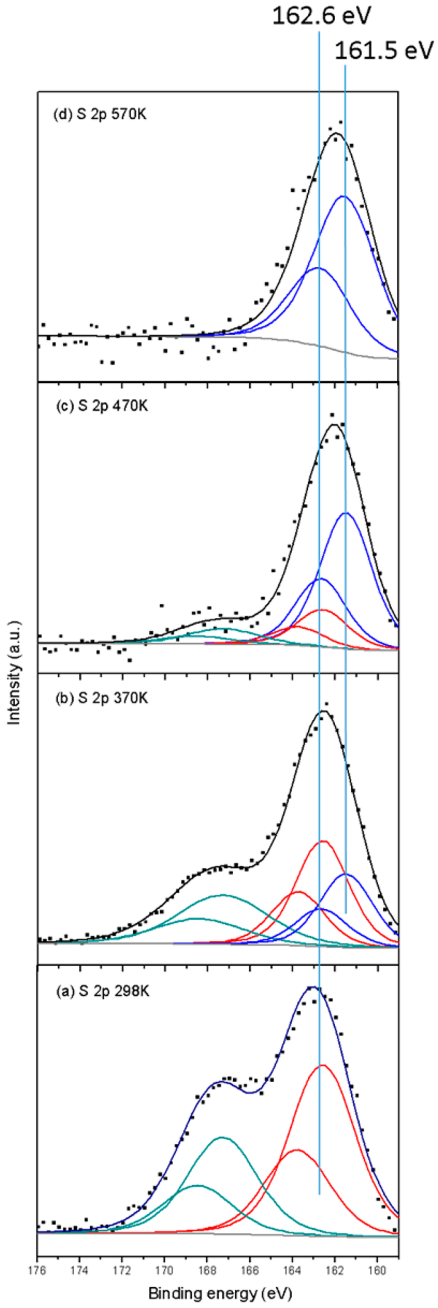

Figure 6. XPS spectra for S 2p from dithiol ligated copper clusters supported on HOPG at varied temperature: (a) 298 K; (b) 370 K; (c) 470 K; (d) 570 K. Black dots are the experimental data. Different deconvoluted oxidation states are marked with different colors. Each oxidation state has two spin−orbit splitting components with a same color. The black line is the overall fitting curve. The light blue vertical lines marks the binding energies of the two critical oxidation states.

that the atomic sulfur atoms that bind to copper is the only version of sulfur left behind. In this dithiol copper cluster system, the evolution of sulfur oxidation states agrees with the studies on alkanethiol copper single crystal systems.[24,25] In those studies, similar binding energies were identified for different sulfur species, such as Cu−S−R at 162.4 eV and Cu−S at 161.5 eV.[24] Unlike the XPS analysis on single crystals, the C 1s signal from the carbon chain is not shown here, because it is overwhelmed by the strong graphene carbon signal due to the HOPG substrate.

DOI: 10.1021/acs.jpcc.7b10452
J. Phys. Chem. C 2018, 122, 2173−2183

It would be interesting to know how well 1,6-hexanedithiol can protect the copper clusters from oxidation under ambient environment. In fact, when exposed to air, the oxidation process can be partially hindered by the dithiol ligands, as demonstrated in Figure 7. The relatively lower intensity of

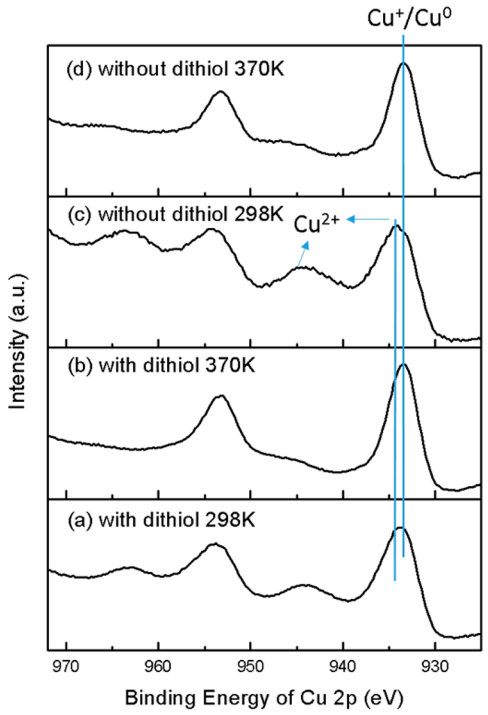

Figure 7. XPS spectra for Cu 2p from dithiol ligated copper clusters and bare copper clusters at varied temperature: (a) ligated clusters at 298 K; (b) ligated clusters after being annealled at 370 K; (c) bare clusters at 298 K; (d) bare clusters after being annealled at 370 K. The blue verticle lines mark the shift of peak position for Cu $2p_{3/2}$. The blue arrows mark the import features for Cu^{2+}.

satellite peaks and slightly lower binding energy for Cu $2p_{3/2}$ at 933.8 eV in Figure 7a compared to Figure 7c (Cu $2p_{3/2}$ at 934.2 eV), confirm the reduced formation of CuO in the dithiol ligated clusters. Note also that the peak shape in Figure 7c implies full oxidation to CuO. Since copper sulfur interaction is fairly strong, it is speculated that dithiol may occupy most of the reactive sites on the copper clusters, thus increasing the reaction barrier for oxygen to oxidize the copper clusters afterward. These results agree with the copper single crystal studies.[25] Davies et al. have demonstrated that oxygen chemisorption on Cu(110) occurs at low methyl mercaptide coverage but can be completely inhibited at high methyl mercaptide coverage under UHV.[25] Formed via LNMD method, dithiol ligated copper clusters in our system can be seen as alkanethiol chemisorbed to copper single crystal surfaces in the high coverage scenario. However, only partial, rather than complete, inhibition of oxidation was seen, likely due to 1. 1,6-hexanedithiol has a long carbon chain, with both ends anchoring to a copper cluster and a relatively bulky bridge structure, preventing active sites from being fully saturated by dithiol; 2. Clusters as small as Cu_{100} are more reactive than copper single crystal surfaces in terms of oxidation reactions; 3. Exposure to ambient pressure is a more severe oxidative situation than dosing oxygen into a UHV chamber.

XPS measurements for Cu 2p at varied temperature are also shown in Figure 7. Unlike the gradual evolution of sulfur oxidation states from 298 to 570 K, the major change for Cu happened immediately when heated up to 370 K. By comparing Figure 7b to a, it is obvious that the satellite peaks of Cu^{2+} have almost disappeared upon heating. Moreover, the Cu $2p_{3/2}$ peak at 370 K becomes narrower, implying fewer oxidation states; and shifts to a lower binding energy (933.5 eV), indicating the dominance of low oxidation states (Cu^{+} or Cu^{0}). Further annealing to 470 K and then 570 K only shifted the peak to a slightly lower binding energy of 933.4 eV (data not shown here). By comparing Figure 7d to c, it is apparent that, without dithiol ligands, Cu^{2+} still get reduced when heated up to 370 K. In fact, heating under UHV is a quite reductive environment for many metal oxides. For example, White et al. have found that for partially oxidized Cu films, CuO gets reduced to Cu_2O at around 380 K.[53] In this sense, the reduction shown in Figure 7b is assigned to the thermally induced reduction instead of the ligation-induced reduction.

Very similar evolutions of sulfur oxidation states and copper oxidation states were seen for varied sizes of copper clusters. Upon ramping to 298 K, it is more likely that dithiol molecules are only ligated to the surface of the copper clusters to form dithiol ligated copper clusters. Therefore, it is expected that the S/Cu ratios should be different among varied cluster sizes. The S/Cu ratios were calculated using the integrated area and then normalized by relative sensitivity factors (sulfur: 0.668, copper: 5.321). As is shown in Figure 8, the smaller the clusters, the

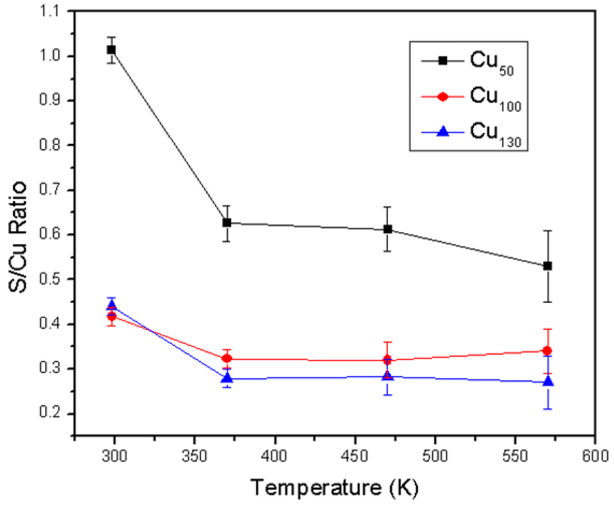

Figure 8. S/Cu ratios of varied cluster sizes and varied temperatures as implied in the graph.

larger the S/Cu ratios. The S/Cu ratios of dithiol ligated Cu_{130} and Cu_{100} clusters are quite close to each other; however, when the cluster size decreases to 50, the S/Cu ratio increases dramatically. It is also worth noticing that no matter the size of the copper clusters, S/Cu ratios always decrease upon annealing, but not by more than half of the initial value. This is due to the bifunctional nature of 1,6-hexanedithiol. Recall the studies of monothiol on copper single crystal which showed that the sulfur XPS signal almost did not change after annealing.[25] This means that any sulfur atoms that have already bound to copper should not desorb upon heating and then cause the S/Cu ratio to decrease. In this sense, the dangling dithiol motif, which is believed to evolve monothiol

DOI: 10.1021/acs.jpcc.7b10452
J. Phys. Chem. C 2018, 122, 2173−2183

based on the TPD data, should be the only source of sulfur loss. It should be also mentioned that some dangling thiol groups may be oxidized or bind to the partially oxidized copper clusters, as is indicated in Figure 6 (a). However, in neither of these two situations do the sulfur atoms bind directly to the copper atoms. In this sense, the unattached thiol groups on the dangling ligands should eventually cause the S/Cu ratio to decrease, regardless of whether they are oxidized or not. If the thiol groups are somehow oxidized and also attached to the partially oxidized copper clusters, the disproportionation reaction, which can happen upon heating, may also cause some fraction of sulfur to be left on the copper clusters.[54] However, the overall differences in the evolution of S/Cu ratio between the Cu_{50} and the Cu_{100} are mainly caused by the ratio of sulfur atoms that actually bind to the surface of the copper clusters. Therefore, it is very likely that these differences are mainly caused by the size effect.

Based on the initial and final S/Cu ratios and the assumption that dangling dithiol ligands should be the only source of sulfur loss, the numbers of dangling and bidentate dithiol ligands per copper cluster can be estimated. As is shown in Table 1, for the total numbers of dithiol ligands, it may be surprising that a Cu_{50} cluster has even more ligands than a Cu_{100} cluster. However, if we take a further comparison between the numbers of dangling and bidentate ligands, it is actually fairly reasonable. For Cu_{50}, nearly all of the dithiol ligands are dangling; however, for Cu_{100}, the majority of the dithiol ligands are bidentate. Unlike a dangling dithiol which needs only one binding site, a bidentate dithiol must occupy two binding sites. Moreover, the bidentate dithiol ligands have a bridge structure with larger steric hindrance, thus likely blocking some of the binding sites. Additionally, it is likely that a smaller cluster, such as Cu_{50}, tends to have more dangling dithiol ligands, while a larger cluster, such as Cu_{100}, tends to have more bidentate dithiol ligands. As a result, with more bidentate dithiol molecules binding to a Cu_{100} cluster, it ends up with fewer dithiol ligands compared to a Cu_{50} cluster. The structural properties of Cu_{50} and Cu_{100} clusters have been reported using Monte Carlo simulations.[55] According to this study, there are 37 surface atoms for Cu_{50} and 65 surface atoms for Cu_{100}.[55] Based on these numbers, the surface S/Cu ratios for Cu_{50} and Cu_{100} are estimated to be 70% and 50%, respectively.

Table 1. Estimated Ligand Numbers of Cu_{50} and Cu_{100} Clusters

total number of copper atoms	50	100
total number of dithiol ligand	25	21
number of dangling dithiol ligand	24	8
number of bidentate dithiol ligand	1	13

CONCLUSION

This work highlights a unique method to synthesize and analyze small ligated metal clusters. The mass-selected soft-landing method makes it efficient to prepare small copper clusters of desired size. The LNMD method can limit the cluster−cluster interactions and maximize the opportunity for dithiol molecules to ligate to the copper clusters. The as-prepared dithiol ligated copper clusters supported on HOPG can be further analyzed though TPD and XPS.

This work has also filled a gap of cluster size in the field previously studied for the copper alkanethiol system. Copper single crystals have been serving as the model system to study copper thiol interactions, and simple short chain monothiols have been the major thiol candidates. This work focuses on the interactions between small copper clusters (i.e., Cu_{100}) and a six-membered bifunctional dithiol (1,6-hexanedithiol). The TPD profiles have shown interesting properties of how 1,6-hexanedithiol ligate and decompose on the small copper clusters. Two different binding motifs (dangling and bidentate) of dithiol ligands have been proposed. Upon heating, three different thiol or hydrocarbon products evolve though C−S bond scission. A monothiol is ascribed to evolve from the dangling motif. Hexane and cyclohexane are assigned to evolve from the bidentate motif though hydrogen recombination and intramolecular coupling respectively. Temperature dependent XPS measurements have revealed a similar evolution of the sulfur oxidation states to that of the copper single crystal studies. XPS measurements have also shown that, after being exposed to air, the dithiol ligands can partially protect the copper clusters from being oxidized.

This work offers a fundamental understanding of the interactions between small copper clusters and bifunctional 1,6-hexandithiol molecules, which may be useful in designing the building blocks of 2-D functional materials.

AUTHOR INFORMATION

Corresponding Author

*E-mail: kbowen@jhu.edu.

ORCID

Linjie Wang: 0000-0002-6558-1753

Kit H. Bowen: 0000-0002-2858-6352

Notes

The authors declare no competing financial interest.

ACKNOWLEDGMENTS

This work was supported by the Office of Naval Research's (ONR) Multidisciplinary University Research Initiative (MURI) under Grant Number N00014-15-1-2681.

REFERENCES

(1) Vajda, S.; White, M. G. Catalysis Applications of Size-Selected Cluster Deposition. *ACS Catal.* **2015**, *5*, 7152−7176.

(2) Cox, D. M.; Eberhardt, W.; Fayet, P.; Fu, Z.; Kessler, B.; Sherwood, R. D.; Sondericker, D.; Kaldor, A. Electronic Structure of Deposited Monosized Metal-Clusters. *Z. Phys. D: At., Mol. Clusters* **1991**, *20*, 385−386.

(3) Bonanni, S.; Ait-Mansour, K.; Harbich, W.; Brune, H. Effect of the TiO_2 Reduction State on the Catalytic CO Oxidation on Deposited Size-Selected Pt Clusters. *J. Am. Chem. Soc.* **2012**, *134*, 3445−3450.

(4) von Weber, A.; Baxter, E. T.; White, H. S.; Anderson, S. L. Cluster Size Controls Branching between Water and Hydrogen Peroxide Production in Electrochemical Oxygen Reduction at Pt_n/ITO. *J. Phys. Chem. C* **2015**, *119*, 11160−11170.

(5) Wörz, A. S.; Judai, K.; Abbet, S.; Heiz, U. Cluster Size-dependent Mechanisms of the CO + NO Reaction on Small Pd_n ($n \leq 30$) Clusters on Oxide Surfaces. *J. Am. Chem. Soc.* **2003**, *125*, 7964−7970.

(6) Wang, B.; Yoon, B.; König, M.; Fukamori, Y.; Esch, F.; Heiz, U.; Landman, U. Size-Selected Monodisperse Nanoclusters on Supported Graphene: Bonding, Isomerism, and Mobility. *Nano Lett.* **2012**, *12*, 5907−5912.

(7) Kwon, G.; Ferguson, G. A.; Heard, C. J.; Tyo, E. C.; Yin, C. R.; DeBartolo, J.; Seifert, S.; Winans, R. E.; Kropf, A. J.; Greeley, J.; et al. Size-Dependent Subnanometer Pd Cluster (Pd_4, Pd_6, and Pd_{17}) Water Oxidation Electrocatalysis. *ACS Nano* **2013**, *7*, 5808−5817.

DOI: 10.1021/acs.jpcc.7b10452
J. Phys. Chem. C 2018, 122, 2173−2183

(8) Lei, Y.; Mehmood, F.; Lee, S.; Greeley, J.; Lee, B.; Seifert, S.; Winans, R. E.; Elam, J. W.; Meyer, R. J.; Redfern, P. C.; et al. Increased Silver Activity for Direct Propylene Epoxidation via Subnanometer Size Effects. *Science* **2010**, *328*, 224−228.
(9) Molina, L. M.; Lee, S.; Sell, K.; Barcaro, G.; Fortunelli, A.; Lee, B.; Seifert, S.; Winans, R. E.; Elam, J. W.; Pellin, M. J.; et al. Size-dependent Selectivity and Activity of Silver Nanoclusters in the Partial Oxidation of Propylene to Propylene Oxide and Acrolein: A Joint Experimental and Theoretical Study. *Catal. Today* **2011**, *160*, 116−130.
(10) Vajda, S.; Lee, S.; Sell, K.; Barke, I.; Kleibert, A.; von Oeynhausen, V.; Meiwes-Broer, K. H.; Rodriguez, A. F.; Elam, J. W.; Pellin, M. M.; et al. Combined Temperature-Programmed Reaction and In-situ X-ray Scattering Studies of Size-selected Silver Clusters under Realistic Reaction Conditions in the Epoxidation of Propene. *J. Chem. Phys.* **2009**, *131*, 121104.
(11) Lee, S. S.; Fan, C. Y.; Wu, T. P.; Anderson, S. L. CO Oxidation on Au-n/TiO2 Catalysts Produced by Size-selected Cluster Deposition. *J. Am. Chem. Soc.* **2004**, *126*, 5682−5683.
(12) Tong, X.; Benz, L.; Kemper, P.; Metiu, H.; Bowers, M. T.; Buratto, S. K. Intact Size-selected Au_n Clusters on a $TiO_2(110)$-(1 × 1) Surface at Room Temperature. *J. Am. Chem. Soc.* **2005**, *127*, 13516−13518.
(13) Tang, X.; Schneider, J.; Dollinger, A.; Luo, Y.; Wörz, A. S.; Judai, K.; Abbet, S.; Kim, Y. D.; Gantefor, G. F.; Fairbrother, D. H.; et al. Very Small "Window of Opportunity" for Generating CO Oxidation-active Au_n on TiO_2. *Phys. Chem. Chem. Phys.* **2014**, *16*, 6735−6742.
(14) Lee, S.; Molina, L. M.; López, M. J.; Alonso, J. A.; Hammer, B.; Lee, B.; Seifert, S.; Winans, R. E.; Elam, J. W.; Pellin, M. J.; et al. Selective Propene Epoxidation on Immobilized Au_{6-10} Clusters: The Effect of Hydrogen and Water on Activity and Selectivity. *Angew. Chem.* **2009**, *121*, 1495−1499.
(15) Liu, C.; Yang, B.; Tyo, E.; Seifert, S.; DeBartolo, J.; von Issendorff, B.; Zapol, P.; Vajda, S.; Curtiss, L. A. Carbon Dioxide Conversion to Methanol over Size-Selected Cu_4 Clusters at Low Pressures. *J. Am. Chem. Soc.* **2015**, *137*, 8676−8679.
(16) Kiskinova, M.; Goodman, D. W. Modification of Chemisorption Properties by Electronegative Adatoms: H_2 and CO on Chlorided, Sulfided, and Phosphided Ni(100). *Surf. Sci.* **1981**, *108*, 64−76.
(17) Moon, D. W.; Bernasek, S. L.; Lu, J. P.; Gland, J. L.; Dwyer, D. J. Activation of Carbon Monoxide on Clean and Sulfur Modified Fe(100). *Surf. Sci.* **1987**, *184*, 90−108.
(18) Kiskinova, M. P. Electronegative Additives and Poisoning in Catalysis. *Surf. Sci. Rep.* **1988**, *8*, 359−402.
(19) Sexton, B. A.; Nyberg, G. L. A Vibrational and TDS Study of Sulfur Adsorbates on Cu(100): Evidence for CH_3S Species. *Surf. Sci.* **1986**, *165*, 251−267.
(20) Mullins, D. R.; Lyman, P. F. Adsorption and Reaction of Methanethiol on W(001). *J. Phys. Chem.* **1993**, *97*, 9226−9232.
(21) Mullins, D. R.; Lyman, P. F. The Adsorption and Reaction of Methanethiol on Ru(0001). *J. Phys. Chem.* **1993**, *97*, 12008−12013.
(22) Donev, S.; Brack, N.; Paris, N. J.; Pigram, P. J.; Singh, N. K.; Usher, B. F. Surface Reactions of 1-Propanethiol on GaAs(100). *Langmuir* **2005**, *21*, 1866−1874.
(23) Kariapper, M. S.; Grom, G. F.; Jackson, G. J.; McConville, C. F.; Woodruff, D. P. Characterization of Thiolate Species Formation on Cu(111) Using Soft X-ray Photoelectron Spectroscopy. *J. Phys.: Condens. Matter* **1998**, *10*, 8661−8670.
(24) Lai, Y. H.; Yeh, C. T.; Cheng, S. H.; Liao, P.; Hung, W. H. Adsorption and Thermal Decomposition of Alkanethiols on Cu(110). *J. Phys. Chem. B* **2002**, *106*, 5438−5446.
(25) Carley, A. F.; Davies, P. R.; Jones, R. V.; Harikumar, K. R.; Roberts, M. W.; Welsby, C. J. A Combined XPS/STM and TPD Study of the Chemisorption and Reactions of Methyl Mercaptan at a Cu(110) Surface. *Top. Catal.* **2003**, *22*, 161−172.
(26) Prince, N. P.; Seymour, D. L.; Woodruff, D. P.; Jones, R. G.; Walter, W. The Structure of Mercaptide on Cu(111): a Case of Molecular Adsorbate-Induced Substrate Reconstruction. *Surf. Sci.* **1989**, *215*, 566−576.
(27) Anderson, S. E.; Nyberg, G. L. UPS of Thiols and Disulfides Adsorbed on Cu(410): CH_3SH, C_2H_5SH, C_3H_7SH, $(CH3S)_2$, $(C_2H_5S)_2$, $(C_3H_7S)_2$. *J. Electron Spectrosc. Relat. Phenom.* **1990**, *52*, 735−746.
(28) Rieley, H.; Kendall, G. K.; Chan, A.; Jones, R. G.; Ludecke, J.; Woodruff, D. P.; Cowie, B. C. C. Surface Adsorption Structures in 1-octanethiol Self-assembled on Cu(111). *Surf. Sci.* **1997**, *392*, 143−152.
(29) Mott, D.; Yin, J.; Engelhard, M.; Loukrakpam, R.; Chang, P.; Miller, G.; Bae, I. T.; Das, N. C.; Wang, C. M.; Luo, J.; et al. From Ultrafine Thiolate-Capped Copper Nanoclusters toward Copper Sulfide Nanodiscs: A Thermally Activated Evolution Route. *Chem. Mater.* **2010**, *22*, 261−271.
(30) Her, J.; Cho, D.; Lee, C. S. Synthesis of Conductive Nano Ink Using 1-Octanethiol Coated Copper Nano Powders in 1-Octanol for Low Temperature Sintering Process. *Mater. Trans.* **2013**, *54*, 599−602.
(31) Huertos, M. A.; Cano, I.; Bandeira, N. A. G.; Benet-Buchholz, J.; Bo, C.; van Leeuwen, P. W. N. M. Phosphinothiolates as Ligands for Polyhydrido Copper Nanoclusters. *Chem. - Eur. J.* **2014**, *20*, 16121−16127.
(32) Dong, T. Y.; Wu, H. H.; Lin, M. C. Superlattice of Octanethiol-Protected Copper Nanoparticles. *Langmuir* **2006**, *22*, 6754−6756.
(33) Wang, Y. W.; Im, J. S.; Soares, J. W.; Steeves, D. M.; Whitten, J. E. Thiol Adsorption on and Reduction of Copper Oxide Particles and Surfaces. *Langmuir* **2016**, *32*, 3848−3857.
(34) Vajda, S.; Pellin, M. J.; Greeley, J. P.; Marshall, C. L.; Curtiss, L. A.; Ballentine, G. A.; Elam, J. W.; Catillon-Mucherie, S.; Redfern, P. C.; Mehmood, F.; et al. Subnanometre Platinum Clusters as Highly Active and Selective Catalysts for the Oxidative Dehydrogenation of Propane. *Nat. Mater.* **2009**, *8*, 213−216.
(35) Barnes, A. J. Molecular Complexes of the hydrogen Halides Studied by Matrix-Isolation Infrared Spectroscopy. *J. Mol. Struct.* **1983**, *100*, 259−280.
(36) Kudoh, S.; Onoda, K.; Takayanagi, M.; Nakata, M. N_2O Clusters in a Supersonic Jet Studied by Matrix-Isolation Infrared Spectroscopy and Density Functional Theory Calculation. *J. Mol. Struct.* **2000**, *524*, 61−68.
(37) Goldberg, N.; Almond, M. J.; Ogden, J. S.; Cannady, J. P.; Walsh, R.; Becerra, R. The Gas-Phase Reactions of $SiCl_4$ and Si_2Cl_6 with CH_3OH and C_2H_5OH: An Investigation by Mass Spectrometry and Matrix-Isolation Infrared Spectroscopy. *Phys. Chem. Chem. Phys.* **2004**, *6*, 3264−3270.
(38) Tsao, M. L.; Zhu, Z. D.; Platz, M. S. Matrix and Time-Resolved Infrared Spectroscopy of Chloro-p-nitrophenylcarbene and Related Species. *J. Phys. Chem. A* **2001**, *105*, 8413−8416.
(39) Teng, Y. L.; Xu, Q. Reactions of Group 14 Metal Atoms with Acetylene: A Matrix Isolation Infrared Spectroscopic and Theoretical Study. *J. Phys. Chem. A* **2009**, *113*, 12163−12170.
(40) Teng, Y. L.; Xu, Q. Reactions of Yttrium and Scandium Atoms with Acetylene: A Matrix Isolation Infrared Spectroscopic and Theoretical Study. *J. Phys. Chem. A* **2010**, *114*, 9069−9073.
(41) Gong, Y.; Andrews, L.; Chen, M. Y.; Dixon, D. A. Reactions of Late Lanthanide Metal Atoms and Methanol in Solid Argon: A Matrix Isolation Infrared Spectroscopic and Theoretical Study. *J. Phys. Chem. A* **2011**, *115*, 14581−14592.
(42) Wang, G. J.; Zhuang, J.; Zhou, M. F. Matrix Isolation Infrared Spectroscopic and Theoretical Study of the Reactions of Tantalum Oxide Molecules with Methanol. *J. Phys. Chem. A* **2011**, *115*, 8623−8629.
(43) Zhao, Y. Y. C-Cl Activation by Group IV Metal Oxides in Solid Argon Matrixes: Matrix Isolation Infrared Spectroscopy and Theoretical Investigations of the Reactions of MO_x (M = Ti, Zr; x = 1, 2) with CH_3Cl. *J. Phys. Chem. A* **2013**, *117*, 5664−5674.
(44) Li, Z. J.; Fang, Z. T.; Kelley, M. S.; Kay, B. D.; Rousseau, R.; Dohnalek, Z.; Dixon, D. A. Ethanol Conversion on Cyclic $(MO_3)_3$ (M = Mo, W) Clusters. *J. Phys. Chem. C* **2014**, *118*, 4869−4877.
(45) Tang, X.; Li, X.; Wang, Y.; Wepasnick, K.; Lim, A.; Fairbrother, D. H.; Bowen, K. H.; Mangler, T.; Noessner, S.; Wolke, C.; et al. Size Selected Clusters on Surfaces. *J. Phys. Conf. Ser.* **2013**, *438*, 012005.

DOI: 10.1021/acs.jpcc.7b10452
J. Phys. Chem. C 2018, 122, 2173−2183

(46) Smith, K. L.; Black, K. M. Characterization of the Treated Surfaces of Silicon Alloyed Pyrolytic Carbon and SiC. *J. Vac. Sci. Technol., A* **1984**, *2*, 744−747.
(47) Müller, T.; Flynn, G. W.; Mathauser, A. T.; Teplyakov, A. V. Temperature-Programmed Desorption Studies of n-Alkane Derivatives on Graphite: Desorption Energetics and the Influence of Functional Groups on Adsorbate Self-assembly. *Langmuir* **2003**, *19*, 2812−2821.
(48) Tang, X.; Bumueller, D.; Lim, A.; Schneider, J.; Heiz, U.; Gantefor, G.; Fairbrother, D. H.; Bowen, K. H. Catalytic Dehydration of 2-Propanol by Size-Selected $(WO_3)_n$ and $(MoO_3)_n$ Metal Oxide Clusters. *J. Phys. Chem. C* **2014**, *118*, 29278−29286.
(49) Doronin, M.; Bertin, M.; Michaut, X.; Philippe, L.; Fillion, J. H. Adsorption Energies and Prefactor Determination for CH_3OH Adsorption on Graphite. *J. Chem. Phys.* **2015**, *143*, 084703.
(50) Teran Arce, F.; Vela, M. E.; Salvarezza, R. C.; Arvia, A. J. Comparative Study of Thiol Films on C(0001) and Au(111) Surfaces by Scanning Probe Microscopy. *Surf. Rev. Lett.* **1997**, *4*, 637−649.
(51) Floro, J. A.; Chason, E.; Cammarata, R. C.; Srolovitz, D. J. Physical Origins of Intrinsic Stresses in Volmer-Weber Thin Films. *MRS Bull.* **2002**, *27*, 19−25.
(52) Kwon, S.; Russell, J.; Zhao, X. C.; Vidic, R. D.; Johnson, J. K.; Borguet, E. Combined Experimental and Theoretical Investigation of Polar Organic Adsorption/Desorption from Model Carbonaceous Surfaces: Acetone on Graphite. *Langmuir* **2002**, *18*, 2595−2600.
(53) Lee, S. Y.; Mettlach, N.; Nguyen, N.; Sun, Y. M.; White, J. M. Copper Oxide Reduction through Vacuum Annealing. *Appl. Surf. Sci.* **2003**, *206*, 102−109.
(54) Alemozafar, A. R.; Guo, X. C.; Madix, R. J. Adsorption and Reaction of Sulfur Dioxide with Cu(110) and Cu(110)-p(2 × 1)-O. *J. Chem. Phys.* **2002**, *116*, 4698.
(55) Dugan, N.; Erkoc, S. Structural Properties of Copper Nanoparticles: Modified Diffusion Monte Carlo Simulations. *Int. J. Mod. Phys. A* **2006**, *17*, 1171−1177.

DOI: 10.1021/acs.jpcc.7b10452
J. Phys. Chem. C 2018, 122, 2173−2183